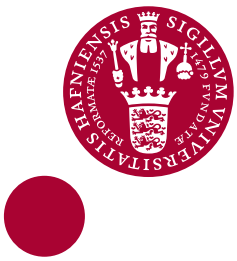

Quasar Elemental Abundances at High Redshifts

Dietrich, M.; Hamann, F.; Shields, J. C.; Constantin, A.; Heidt, J.; Jaeger, K.; Vestergaard, Marianne; Wagner, S. J.

Published in:
Astrophysical Journal

DOI:
10.1086/374662

Publication date:
2003

Quasar Elemental Abundances at High Redshifts

M. Dietrich [1,2], F. Hamann [1], J.C. Shields [3], A. Constantin [3], J. Heidt [4], K. Jäger [5], M. Vestergaard [6], and S.J. Wagner [4],
dietrich@chara.gsu.edu

ABSTRACT

We examine rest-frame ultraviolet spectra of 70 high redshift quasars ($z \geq 3.5$) to study the chemical enrichment history of the gas closely related to the quasars, and thereby estimate the epoch of first star formation. The fluxes of several ultraviolet emission lines were investigated within the framework of the most recent photoionization models to estimate the metallicity of the gas associated with the high-z quasars. Standard photoionization parameters and the assumption of secondary nitrogen enrichment indicate an average abundance of $Z/Z_\odot \simeq 4$ to 5 in the line emitting gas. Assuming a time scale of $\tau_{evol} \simeq 0.5 - 0.8\,\mathrm{Gyrs}$ for the chemical enrichment of the gas, the first major star formation for quasars with $z \simeq 4$ should have started at a redshift of $z_f \simeq 6 - 8$, corresponding to an age of the universe of several $10^8\,\mathrm{yrs}$ ($H_o = 65\ \mathrm{km\,s^{-1}\,Mpc^{-1}}$, $\Omega_M = 0.3$, $\Omega_\Lambda = 0.7$). We note that this also appears to be the era of re-ionization of the universe. Finally, there is some evidence for a positive luminosity – metallicity relation in this high redshift quasar sample.

1. Introduction

Quasars at high redshift are excellent tools to investigate the formation of galaxies and supermassive black holes in the early universe, and to probe the physical state of their galactic environment up to early cosmic epochs. In recent years there is growing evidence that quasar activity and the formation of their host galaxies, in particular of massive spheroidal systems, are closely related.

The presence of dark massive objects (DMOs) in the center of nearly every galaxy with a significant spheroidal component supports models that connect the formation and evolution of galaxies with quasar activity. It has been shown that the mass of the DMOs, generally regarded as supermassive black holes, is closely correlated with the spheroidal mass of the host-galaxy (e.g., Kormendy & Richstone 1995; Magorrian et al. 1998; Richstone et al. 1998; Gebhardt et al. 2000; Merritt & Ferrarese 2001; Tremaine et al. 2002). In the context of galaxy evolution, the conditions that give rise to quasars and massive black holes will also yield solar or super-solar metallicities on time scales shorter than $\sim 1\,\mathrm{Gyr}$ (Arimoto & Yoshii 1987; Hamann & Ferland 1993; Gnedin & Ostriker 1997; Friaça & Terlevich 1998; Cen & Ostriker 1999; Romano et al. 2002). Additional strong evidence for the relationship between quasar activity, host galaxy formation, and intense star formation episodes is provided by the detection of large amounts of dust ($\sim 10^8\,\mathrm{M_\odot}$) and molecular gas ($\sim 10^{10}\,\mathrm{M_\odot}$) measured in high redshift quasars (Andreani, La Franca, & Cristiani 1993; Isaak et al. 1994; Omont et al. 1996, 2001; Carilli et al. 2000, 2001). The co-moving number density of quasars and the cosmic star formation rate are both at least one order of magnitude larger for epochs with $z \gtrsim 1$ than in the local universe

[1]Department of Astronomy, University of Florida, 211 Bryant Space Science Center, Gainesville, FL 32611-2055, USA.

[2]current address: Department of Physics and Astronomy, Georgia State University, One Park Place South SE, Atlanta, GA 30303, USA.

[3]Department of Physics and Astronomy, Ohio University, Athens, OH 45701, USA.

[4]Landessternwarte Heidelberg–Königstuhl, Königstuhl 12, D–69117 Heidelberg, Germany.

[5]Universitätssternwarte Göttingen, Geismarlandstraße 11, D–37083 Göttingen, Germany.

[6]Department of Astronomy, The Ohio State University, 140 West 18th Av., Columbus, OH 43210-1173, USA.

(e.g., Gallego et al. 1995; Lilly et al. 1996; Connolly et al. 1997; Tresse & Maddox 1998; Steidel et al. 1999; Lanzetta et al. 2002). The evolution of the space densities of quasars and galaxies with starburst activity are also very similar. Finally, there may be a relation between the luminosity functions of normal galaxies and quasars (e.g., Dickinson 1998; Pettini et al. 1998; Boyle & Terlevich 1998).

Quasars at high redshift are therefore of interest as valuable probes to date the beginning of the first star formation episodes in the early universe (Hamann & Ferland 1992, 1993, 1999; Dietrich et al. 1999, 2000). Currently, about 350 quasars with redshifts $z \geq 4$ are known (e.g., Schneider et al. 1991a, b; Storrie-Lombardi et al. 1996; Anderson et al. 2001; Djorgovski 2002), and several quasars with $z \gtrsim 5$ and even $z > 6$ have been recently discovered (Fan et al. 1999, 2000a, b, 2001; Stern et al. 2000; Zheng et al. 2000; Sharp et al. 2001; Becker et al. 2001). The redshift range $z \gtrsim 4$ corresponds to an epoch when the universe was less than $\sim 10\,\%$ of its current age ($H_o = 65$ km s^{-1} Mpc^{-1}, $\Omega_M = 0.3$, $\Omega_\Lambda = 0.7$; Carroll, Press, & Turner 1992).

The chemical composition of the gas associated with quasars can be estimated using the broad emission lines in the ultraviolet spectral range (for a review, see Hamann & Ferland 1999). Unfortunately, the strengths of prominent metal lines, such as C IVλ1549, relative to Lyα are not sensitive to the overall metallicity for $Z \gtrsim 0.1 Z_\odot$ (Hamann & Ferland 1999). Shields (1976) proposed that the relative nitrogen abundance could be used as an indirect metallicity indicator. Assuming that the secondary nitrogen production, i.e., the synthesis of nitrogen from existing carbon and oxygen via CNO burning in intermediate mass stars (Tinsley 1980; Henry et al. 2000), is the dominant source for nitrogen, this results in $N/O \propto O/H$ and hence $N/H \propto (O/H)^2 \propto Z^2$. Observations of HII regions indicate that secondary nitrogen production and the $N/O \propto O/H$ scaling dominate when the metallicity is above $\sim 1/3$ to $\sim 1/2$ solar (Shields 1976; Pagel & Edmunds 1981; van Zee et al. 1998; Izotov & Thuan 1999; Pettini et al. 2002). It has been noted (Henry et al. 2000; Kobulnicky & Skillman 1996) that departures from the simple $N/O \propto O/H$ relationship can occur if the enrichment is dominated by star formation in discrete bursts. This situation leads to time-dependent fluctuations in the N/O ratio because of different delays in the stellar release of N and O (and C). However, the overall trend for increasing N/O with O/H remains. Moreover, there are no reports, to our knowledge, of large N/O ratios in metal poor interstellar gas. Large N/O abundances are an indicator of high metallicities in any scenario that involves a well-mixed interstellar medium.

Early investigations of the abundances in broad emission-line region (BELR) gas were based on several generally weak inter-combination lines like N IV]λ1486, O III]λ1663, N III]λ1750, and C III]λ1909 (Shields 1976; Davidson 1977; Baldwin & Netzer 1978; Osmer 1980; Gaskell et al. 1981; Uomoto 1984). The results of these studies already indicated larger than solar metallicity for the BELR gas. Recent studies of high-redshift quasars ($z \gtrsim 3$) provide evidence for significantly enhanced metallicities up to several times solar. These results obtained by studying the emission line properties of quasars (Hamann & Ferland 1992, 1993; Ferland et al. 1996; Dietrich et al. 1999, 2002a; Dietrich & Wilhelm-Erkens 2000; Hamann et al. 2002; Warner et al. 2002) have been corroborated by studies of the intrinsic absorption lines (Petitjean et al. 1994; Møller et al. 1994; Hamann 1997; Pettini 1999). The derived high chemical abundances require an era of major star formation at some earlier epoch.[7]

Hamann & Ferland (1992, 1993) and Ferland et al. (1996) show that emission line ratios involving N Vλ1240 are particularly valuable. Generally, it is observed that N Vλ1240 is stronger than expected in the spectra of high redshift quasars compared to standard photoionization models with solar abundance. Assuming nitrogen scales roughly as Z^2 at solar and higher metallicities Hamann & Ferland (1992, 1993) suggest N Vλ1240/C IVλ1549 and N Vλ1240/He IIλ1640 as valuable metallicity indicators. Recently, Hamann et al. (2002) presented results of a detailed investigation on the influence of the photoionizing continuum flux and spectral shape, density, and metallicity on emission line ratios. They further quantified the metal-

[7] The high metallicities cannot be caused by contamination by single stars or small star clusters. Substantial stellar populations must be involved in the enrichment because the large masses of gas estimated for the BELR require a large mass of heavy elements (Baldwin et al. 2002).

licity and $N/H \propto Z^2$ dependence of various line ratios, including several weak inter-combination lines. They favor N III]λ1750/O III]λ1663 and N Vλ1240/(O VIλ1034 + C IVλ1549) line ratios as the most robust indicators to measure the gas chemical composition.

In section 2 we describe the sample of the $z \gtrsim 3.5$ quasars studied here. In section 3 the results of the analysis of the emission line spectra are presented. We estimate the elemental abundance of the line emitting gas based on several diagnostic emission line ratios (Hamann et al. 2002). Using these emission-line ratios, the mean metallicity is $Z/Z_\odot \simeq 4$ to 5 for the BELR gas of the quasar sample we observed. The results are discussed and compared with previous studies (e.g., Ferland et al. 1996; Hamann & Ferland 1999; Dietrich et al. 1999, 2002a; Dietrich & Wilhelm-Erkens 2000; Hamann et al. 2002; Warner et al. 2002) in section 4. The chemical composition of the BELR gas provides further evidence that the first episodes of major star formation started at a redshift of $z_f \simeq 6$ to 8, corresponding to an age of the universe of several 10^8 years. This result is in good agreement with recent model predictions relating quasar activity with the formation of massive spheroidal systems, e.g., the progenitors of early type galaxies. In the following we assume $H_o = 65$ km s^{-1} Mpc^{-1}, $\Omega_M = 0.3$, $\Omega_\Lambda = 0.7$.

2. High-Redshift Quasar Sample

We have compiled spectra for a sample of 70 high redshift quasars ($3.5 \lesssim z \lesssim 5.0$) to study the chemical composition of the BELR gas and its implications on the star formation history in quasar host galaxies in the early universe.

Most of the quasars at redshift $z \gtrsim 4$ were observed by Constantin et al. (2002). They recorded high signal-to-noise moderate resolution spectra over multiple observing runs at the Multiple Mirror Telescope Observatory (MMT) and the W.M. Keck Observatory. The spectral wavelength range was chosen to cover the redshifted Lyα to He IIλ1640 emission lines. Dietrich et al. (1999, 2002a) observed a small sample of 11 quasars with $z \gtrsim 4$ using FORS 1 at the VLT unit telescope *Antu* in 1998 and 1999. These spectra cover a rest-frame wavelength range of $\sim 850 - 2100$ Å. This wide range allows measurements of not only Lyα up to the He IIλ1640 emission line, but also O VIλ1034, N III]λ1750, and in some cases even C III]λ1909. The high redshift quasar sample was complemented by observations which were kindly provided by Sargent et al. (1988, 1989), Schneider et al. (1991a,b), Storrie-Lombardi et al. (1996), and Steidel & Sargent (unpublished). In particular, the quasar spectra obtained by Storrie-Lombardi et al. (1996) cover the wavelength range containing O VIλ1034 for many of the sources observed by Constantin et al. (2002). Multiple spectra of the same object were combined whenever possible.

Broad-absorption line quasars (BAL QSOs) were excluded from this study, although there are indications that their emission line properties do not differ from non-BAL quasars (Weymann et al. 1991). In Table 1, we list the quasars used in this study together with their redshifts, intrinsic continuum luminosity $L_\lambda(1450\text{Å})$ (corrected for galactic extinction; Dietrich et al. 2002b), the covered restframe wavelength range, and the references for the observations.

3. Analysis

Comparing mean spectra of the $z \gtrsim 4$ quasars with those at $z \simeq 2$ Constantin et al. (2002) found evidence for enhanced N Vλ1240 emission strength in the high-z quasar spectra indicating high metallicities. In the following we present quantitative metallicity estimates for each individual quasar based on several measured emission line ratios.

The quasar spectra were transformed to their restframe using the redshifts listed in Table 1. To determine the redshift for each quasar we fit a Gaussian profile to the upper part of the C IVλ1549 emission line ($I_\lambda \geq 50\,\%$ of the peak intensity).

To measure integrated emission line fluxes, we corrected each quasar spectrum for Fe emission and the weak contribution of Balmer continuum emission while simultaneously obtaining a power-law fit representing the quasar continuum. The power-law fit, $F_\nu \propto \nu^\alpha$, was calculated using small spectral regions, each 10 to 20 Å wide, which are free of detectable emission lines, at $\lambda \simeq 1290$ Å, 1340 Å, 1450 Å, 1700 Å, 1830 Å, and 1960 Å, respectively. To estimate the contribution of the Balmer continuum and Fe line emission,

we used our results from the analysis of quasar composite spectra based on a large quasar sample of about 750 quasars (Dietrich et al. 2002b). For the Balmer continuum emission, we calculated a template spectrum with $T_e = 15\,000\,\mathrm{K}$, $\tau_{BaC} = 1.0$, and $n_e = 10^8\,\mathrm{cm}^{-3}$ following Grandi (1982) and Storey & Hummer (1995). The Fe emission was defined by an empirical template spectrum (Vestergaard & Wilkes 2001) and the results of detailed model calculations (Verner et al. 1999). The empirical emission template accounts for both Fe II and Fe III emission. The spectral width of the Fe emission features was adjusted to the FWHM of the C IVλ1549 emission line profile of each quasar. We found that the strength of the Balmer continuum emission and of the Fe line emission can be estimated as a fraction of the integrated *pseudo continuum* flux in the wavelength range $1420-1470\,$Å. The Balmer continuum emission contributes approximately $1.6\pm0.7\,\%$ and the Fe emission amounts to $1.7\pm0.4\,\%$ (Dietrich et al. 2002b). In spite of this small contributions, the estimate of the Fe line emission improves especially the measurements of N III]λ1750 and lines such as He IIλ1640 near the $\lambda1600\,$Å feature (Laor et al. 1994; Vestergaard & Wilkes 2001).

The C IVλ1549 line profile was fitted with a broad and narrow Gaussian component. The approach to reconstruct the emission line profiles with two Gaussian components was chosen to measure the integrated line flux; however, each individual component has no physical meaning by itself. These components have been used as a template to measure the other emission line fluxes. In using this approach to fit other emission lines, the widths of the broad and narrow component were fixed in velocity space while their strengths were allowed to vary independently. Furthermore, shifts in velocity space of each component were restricted to a range of less than a few $100\,\mathrm{km\,s}^{-1}$ with respect to C IVλ1549. Using the components of the C IVλ1549 emission line as templates is particularly important for measuring N Vλ1240 and He IIλ1640 because they are blended with other emission lines. Furthermore, employing the C IV line profile as a template provides measurements of important weak lines like N III]λ1750 and N IV]λ1486 which are usually difficult to measure. This template-fitting approach is well justified because C IVλ1549, N Vλ1240, and He IIλ1640 are all high ionization lines (HIL). Figure 1 show typical examples of the deblending of the Lyα1216 - N Vλ1240, C IVλ1549 - He IIλ1640 - O III]λ1663, and N III]λ1750 emission line profile complexes, respectively.

The measurement of the N IV]λ1486 emission line flux is severely affected by the blue wing of the broad C IV component. Particularly, for quasars with broad emission line profiles, the N IV]λ1486 line tends to show a low contrast to the outer part of the C IVλ1549 line profile (see Dietrich & Hamann 2003, in prep. for further discussion). The O VIλ1034 emission line flux has been corrected for Lyα forest absorption shortward of the Lyα emission line. For this correction we assumed that the quasars show an intrinsic unabsorbed continuum slope of $\alpha = -1.76$ ($F_\nu \propto \nu^\alpha$) for $\lambda \leq 1200\,$Å, following Telfer et al. (2002). Provided that the same fraction of the continuum and O VIλ1034 emission line flux were absorbed, we estimated a corresponding correction factor. The integrated O VIλ1034 flux was corrected by this factor, which varied from 1.17 to 2.77, with an average of 1.75 ± 0.42.

The uncertainties of the flux measurements were estimated from the multi-component line fit using the scaled C IVλ1549 line profile to obtain a minimum χ^2 of the fit. For the stronger lines like Lyα1216, N Vλ1240, Si IVλ1402, C IVλ1549, and C III]λ1909 the errors are of the order of $\sim 10\,\%$; for the weaker lines, they are $\sim 20-40\,\%$. These errors do not take into account the uncertainties introduced by the placement of the continuum. While the strength of strong emission lines like C IVλ1549 is not changed significantly, the emission line flux of weaker lines like N IV]λ1486 can be underestimated by a factor of as much as ~ 2 (Dietrich & Hamann 2003, in prep.).

4. Results

We calculated emission line ratios relating nitrogen lines with lines of helium, oxygen, and carbon to derive the chemical composition of the BELR gas at high redshifts. These line ratios are used to estimate the chemical abundances employing the results of Hamann et al. (2002). They studied in detail the dependence of emission line ratios from the gas metallicity and the shape of the ionizing continuum. For several metallicities and con-

tinuum shapes, they calculated grids of photoionization models spanning a wide range of density, n_e, and continuum strength, ϕ_H, using CLOUDY (Ferland et al. 1998). The metallicity was varied from $Z/Z_\odot = 0.2$ to 10 with all of the metals scaled in solar ratios, except $N/O \propto Z$. Three different input continua were used — a broken power-law continuum with an UV bump (Mathews & Ferland 1987), a single power-law continuum with $\alpha = -1$, and a segmented power-law that provides the best match to recent observations (Zheng et al. 1997; Laor et al. 1997). For more details of the model calculations, see Hamann et al. (2002).

The gas metallicity as provided by each of the emission line ratios is presented in Figure 2, assuming a segmented power-law continuum. The uncertainties of the emission line flux measurements are propagated for each line ratio and are used to infer an error of each metallicity estimate. The most reliable line ratios are N III]/O III] and N V/(O VI+C IV). In particular, N III]/O III], N V/(O VI+C IV), and N V/C IV provide reasonably consistent results. In spite of some differences, the individual metallicities of all line ratios indicate several times solar metallicity for the line emitting gas close to the quasars at $z \gtrsim 3.5$.[8]

Generally, the estimates of the metallicity based on these ratios are nearly independent of the shape of the photoionizing continuum (Hamann et al. 2002). For comparison, we also estimated metallicities, using each line ratio, which were calculated with a hard power-law continuum ($\alpha = -1.0$) and a SED of the ionizing continuum as suggested by Mathews & Ferland (1987). The derived metallicities differ by less than $\sim 25\,\%$ in most cases. The strongest influence of the input continuum shape is for N V/He II, which amounts to a factor of ~ 2 between the two most different continuum shapes. However, Hamann & Ferland (1993) and Ferland et al. (1996) noted that this line ratio provides a firm lower limit on N/He when adopting BELR parameters that maximize the predicted N V/He II line ratio, e.g., a hard power-law continuum ($\alpha = -1.0$).

[8]Recent investigations of the photospheric solar abundance indicate that carbon and oxygen are about 30 % lower (Holweger 2001; Allende Prieto et al. 2001, 2002) than the values hitherto generally used as solar abundance (Grevesse & Sauval 1998), while the nitrogen abundance remains nearly unchanged within the errors. Hence, this would reduce the derived abundances for the high redshift quasars by $\sim 30\,\%$.

4.1. Comparison of N III], N IV], and N V Metallicity Estimates

Table 2 lists the mean and median metallicities which we derived for each of the individual emission line ratios. To estimate the uncertainty of the mean metallicities inferred for each line ratio, we used the errors of the line ratios which are implied by the individual line flux measurements, σ_{obs} (see section 3). In addition, the width of the distribution of the metallicities based on the corresponding line ratio for each quasar was taken into account using the rms of the mean, i.e., σ_{mean} (Bevington 1969). These both contribution are used in quadrature, i.e., $\sigma = \sqrt{\sigma_{obs}^2 + \sigma_{mean}^2}$, to estimate the errors of the mean metallicities in Table 2.

For 35 of the 70 high-redshift quasars we could compare the chemical abundance based on N III]/O III] and the ratios involving N Vλ1240 (Figure 3). Although N V/C IV, as well as N V/O VI tend to yield higher metallicities than N III]/O III], even this latter line ratio indicates several times solar metallicity. The mean metallicities inferred by N V/C IV, N V/O VI and N V/(O VI+C IV) are only larger by a factor of $\sim$ 1.7, $\sim$ 1.6, and $\sim$ 1.6, respectively, than those derived from N III]/O III] (Table 2). Only a few high redshift quasars differ significantly from the shown trend (Figs. 3a, 3b, and 3c). Hence, emission line ratios involving N III] and N V provide reasonably consistent estimates of the gas metallicity for quasars. The line ratio N V/He II shows the largest difference in the metallicity estimates in comparison with N III]/O III] (Fig. 3d). However, this ratio is particularly sensitive to the uncertain ionizing continuum shape (Hamann et al. 2002). The metallicities we obtained for N V/He II using a hard power-law continuum agree better with the values provided by N III]/O III]. The average metallicity based on N III]/O III] (segmented power-law) and N V/He II based on a hard power-law ($\alpha = -1$) are very similar ($Z/Z_\odot = 3.6 \pm 0.3$ and 2.9 ± 0.4, respectively).

The N III]/C III] ratio tends to indicate lower chemical composition than the other line ratios (Fig. 2), i.e., solar to two times solar metallicity. However, this line ratio is known to be more dependent on the temperature of the gas than

N III]/O III], and the critical densities of N III] and C III] differ by a factor of ~ 2. Hence, N III]/C III] is not as robust as N III]/O III]; emission in N III] and C III] may also occur in spatially different parts of the line emitting region with different physical conditions (Hamann et al. 2002). In addition, the C/O abundance may exhibit a secondary-like behavior at large O/H, similar to, but not as sharply rising as, $N/O \propto O/H$ (Henry et al. 2000). We estimate that, if this C/O behavior was folded into the calculations of Hamann et al. (2002), the metallicities inferred from N III]/C III] would be $\sim$ 2 times larger, while the result based on N V/C IV and N V/(O VI+C IV) would be unchanged (because C IV is already thermalized and a dominant coolant; see Hamann & Ferland 1999), suggesting this effect is probably operating.

Figures 4 and 5 compare the metallicities we calculated based on the remaining line ratios. The metallicities derived from the N V ratios agree reasonably well with each other. For several quasars we could also compare the metallicities inferred by N IV]/O III] with the results obtained using flux ratios including N III] and N V. In Figure 4d the metallicities given by N IV]/O III] are plotted versus those derived from N V/C IV. Although the scatter is quite large, the average metallicities indicated by each line ratio are consistent with $\lesssim 5\,\%$ with each other. The comparison of the metallicities calculated using N IV]/O III] and N III]/O III] are displayed in Figure 5c. The chemical composition indicated by these line ratios is consistent within a factor of $\lesssim 1.7$.

The N IV]/C IV line ratio indicates in general lower metallicities than the other ratios (Figures 2, 5a, 5b, and Table 2). The tendency toward a significantly lower metallicity based on N IV]/C IV was also noted by Shemmer & Netzer (2002). The average metallicity indicated by N IV]/C IV is a factor of $\sim$ 2.5 lower than those given by N V/(O VI+C IV). The physical reason for this difference is hitherto not understood. The metallicity estimates based on N IV]/C IV may appear low in part due to the difficulty in measuring the line flux of the weak N IV]λ1486 emission line. In particular, for quasars with broad emission line profiles the N IV]λ1486 line is located in the outer wing of the C IVλ1549 profile. With a typical strength of about $\sim 5\,\%$ of the C IVλ1549 line flux for solar metallicity, this line can be well hidden in the outer blue wing of C IV. However, a close inspection of the quasar spectra already indicates that not enough flux can be assigned to N IV]λ1486 to achieve a N IV]/C IV line ratio that is consistent with the high metallicities indicated by the other emission line ratios. Another problem with this emission line ratio is that it compares an intercombination (semi-forbidden) line to a strong permitted line, whose optical depths differ by several orders of magnitude. The ratio, therefore, is strongly sensitive to ambiguities in the radiative transfer, e.g., turbulent line broadening.

In Figures 6a and 6b, the mean metallicity based on the N V line ratios is compared with those obtained from line ratios involving intercombination lines. The average metallicity based on N V line ratios indicates higher abundances than those inferred from inter-combination line ratios ($Z/Z_\odot = 6.2 \pm 0.4$ and 3.6 ± 0.4, respectively).

Although a nitrogen overabundance is commonly assumed as the cause of N V enhancement, scattered Lyα and continuum emission by outflowing broad absorption line (BAL) gas clouds would tend to bring the N V and intercombination estimates into better agreement. However, it is still an open question whether all quasars have BAL type outflow that results in absorption lines visible only from certain viewing angles. Several models of an outflowing BAL wind have been studied (Surdej & Hutsemeker 1987; Hamann, Korista, & Morris 1993; Krolik & Voit 1998). Hamann & Korista (1996) found that only a fraction of the N Vλ1240 emission can be ascribed to scattering in the BAL region. They estimate upper limits of $\lesssim 30\,\%$ for N Vλ1240 and $\lesssim 10\,\%$ for C IVλ1549. We used these upper limits to recalculate the emission line ratios involving N V and C IV. The scattered light corrected line ratios indicate chemical compositions which are in better agreement with N III]λ1750/O III]λ1663 (Table 2). Hence, the main result is still valid that the metallicity of the gas closely related to quasars at high redshift is several times solar.

In addition to the mean metallicity based on the individual ratios (Table 2), we calculated the overall mean metallicity of the high-z quasar sample. For each quasar an average metallicity was calculated using the estimates from the line ratios measured in the individual spectra. Furthermore, we have calculated average metallicities for

each quasar based on the inter-combinations lines, as well as on the N V line ratios, only. Table 2 lists the average metallicity calculated using all line ratios available for each quasar. These average overall abundances are plotted as a function of redshift in Figure 7. The overall metallicity for the 70 high redshift quasars is 4 to 5 times solar ($Z/Z_{\odot} = 5.3 \pm 0.3$). It should be kept in mind that all of the metallicity estimates given in this paper would be $\sim 30\,\%$ lower if we used the new solar abundances from Holweger (2001) and Allende Prieto, Lambert, & Asplund (2001, 2002).

4.2. The Metallicity – Luminosity Relationship

We used our quasar sample to test the potential existence of such a $L - Z$ relation at high redshifts. We calculated the rest-frame continuum luminosity for each quasar in our sample, $L_{\lambda}(1450\text{Å})$, at $\lambda = 1450\,\text{Å}$. The investigated high redshift quasars cover a range of $10^{42} \lesssim L_{\lambda}(1450\text{Å}) \lesssim 10^{45}$ erg s^{-1} Å^{-1}. Most of the quasars show a luminosity of $\log L_{\lambda}(1450\text{Å}) \simeq 43\,\text{to}\,44$. In Figure 8, the average metallicity calculated from all ratios in each quasar, is shown as a function of intrinsic continuum luminosity $L_{\lambda}(1450\text{Å})$ for the quasars of our sample. A weak trend of increasing $Z/Z_{\odot}$ toward higher luminosity is visible. We calculated a least square fit to the luminosity – $Z/Z_{\odot}$ distribution shown in Figure 8 (dashed line). The correlation, which shows considerable scatter and spans a small range in luminosity, is marginally significant, with a 6 % probability of arising by chance (70 measurements and correlation coefficient +0.23; Bevington 1969). Although the correlation is not very significant, it provides an additional indication for a luminosity – metallicity (L – $Z/Z_{\odot}$) relation for quasars (Hamann & Ferland 1993, 1999). We are currently in the process of analyzing a sample of ~ 750 quasars in order to study the evolution of their properties, and find for these objects a trend of increasing metallicity with increasing luminosity (Dietrich & Hamann 2003).

5. Discussion

The high metallicities we derived for the BELR gas of the quasars at $z \gtrsim 4$ provide important information about the preceding star formation epoch that is required to enrich the gas. This star formation epoch might also mark the time of the formation of the quasar host galaxies. Several groups have noted that the observed elemental abundances near quasars are consistent with normal chemical enrichment in the cores of massive galaxies. In particular, one-zone chemical evolution models using with a relatively flat IMF (compared to the solar neighborhood) typically achieve supersolar gas-phase metallicities in less than ~ 1 Gyr (e.g., Hamann & Ferland 1992, 1993; Matteucci 1992; Matteucci & Padovani 1993; Padovani & Matteucci 1993). Comparable short times scales for attaining metal rich gas are predicted by more recent multi-zone models that follow the dynamical and chemical evolution of forming galaxies (e.g., Friaça & Terlevich 1998; Granato et al. 2001; Romano et al. 2002). In the multi-zone models, intense star formation on short time scales occurs only in the central region of the quasar host galaxy ($r \lesssim 1$ kpc) and the predicted luminosities of the evolving galaxies are an order of magnitude lower luminosities than the obtained with single-zone models. Super-solar metallicities are predicted to occur within $\tau_{evol} \simeq 0.5 - 0.8$ Gyrs for these central regions (Friaça & Terlevich 1998; Romano et al. 2002).

Based on the timescale for enriching the BELR gas of the high-redshift quasars in this study, the beginning of the first star formation epoch can be estimated. A redshift $z \gtrsim 4$ corresponds to an age of the universe of less than ~ 1.3 Gyrs ($H_o = 65\,\text{km s}^{-1}\,\text{Mpc}^{-1}$, $\Omega_M = 0.3$, $\Omega_{\Lambda} = 0.7$). Assuming $\tau_{evol} \simeq 0.5 - 0.8$ Gyrs for the star formation needed to enrich the gas, the first major star formation epoch started at $z_f \simeq 6 - 8$ for observed quasars at $z \simeq 4.5$. It is interesting to note that this is comparable to the epoch of re-ionization of the universe (Haiman & Loeb 1998; Becker et al. 2001; Fan et al. 2002). These results are also consistent with cosmic structure formation models (Gnedin & Ostriker 1997) which are suggesting that the rapid assembly of (at least some) massive spheroidal systems, accompanied by intense star formation, started at $z_f \simeq 6\,\text{to}\,8$. Assuming that at the end of the major star formation episode in the early phase of galaxy evolution, quasar activity starts in a chemical highly enriched environment (e.g., Granato et al. 2001; Romano et al. 2002) the formation of spheroidal systems might continue until $z \simeq 2$ (Madau et al. 1996; Friaça & Terlevich

1998; Steidel 1999).

The metallicities presented here and by Dietrich et al. (2002a) based on the emission lines in quasars at $z \gtrsim 4$ are consistent with previous emission line studies of $2 \lesssim z \lesssim 4$ quasar samples. In particular, there is no evidence for a decline in the metallicity from $z \simeq 2$ to $z > 4$ (see also Dietrich & Hamann 2003).

In the context of galaxy evolution models, higher metallicities and shorter evolution timescales are expected for more massive stellar systems (Gnedin & Ostriker 1997; Cen & Ostriker 1999; Kauffmann & Haehnelt 2000; Nolan et al. 2001). The close connection of quasars and the formation of massive galaxies is supported by the relation of the black hole mass and the mass of the spheroidal galaxy component (e.g., Gebhardt et al. 2000; Ferrarese & Merritt 2001). For elliptical galaxies, a mass – metallicity relation has been well known for several decades (Sandage 1972; Faber 1973; Bica et al. 1988). Hence, a similar mass – metallicity relation can be expected for quasars. Indeed, there is some evidence for a correlation of metallicity and luminosity, i.e., with the black hole mass of quasars, based on broad emission line studies similar to the analysis we present in this paper (Hamann & Ferland 1993; Shemmer & Netzer 2002; Warner et al. 2003).

6. Conclusion

We investigated rest-frame ultraviolet spectra with moderate spectral resolution of a sample of 70 high redshift quasars with $z \geq 3.5$. We used emission-line flux ratios involving carbon, nitrogen, oxygen, and helium to estimate the metallicity of the line-emitting gas. To transform the observed line ratios into metallicities, we used the results of detailed photoionization calculations as described by Hamann et al. (2002).

A comparison of the gas chemical composition derived from emission line ratios involving N III] and N V indicates reasonable consistent estimates of the gas metallicity. The estimates of the chemical abundances based on N III]/O III] and N V/O VI, N V/(O VI+C IV), and N V/C IV differ by $\sim 50\,\%$. Based on eight individual emission line ratios we estimated an average overall metallicity for the 70 high redshift quasars of roughly $Z/Z_\odot \simeq 4$ to 5. Assuming an upper limit contribution of scattered Lyα emission of $\lesssim 30\,\%$ to the observed N Vλ1240 emission (Hamann & Korista 1996), the average metallicity of the BELR gas at high redshifts is still super-solar, within $\sim 20\,\%$ of the estimate above. Compared to previous studies, we find no evidence for an evolutionary trend in quasar metallicities from $z \simeq 2$ to $z \gtrsim 4$.

We analyze the derived elemental abundances within the context of models presented by Hamann & Ferland (1993) and Friaça & Terlevich (1998). With an evolution time scale of approximately $\tau_{evol} \sim 0.5$ to 0.8 Gyrs, the epoch of the first intense star formation is estimated to begin as early as at a redshift of $z_f \simeq 6$ to 8, i.e., less than 1 Gyr of the age of the universe ($H_o \simeq 65$ km s^{-1} Mpc^{-1}, $\Omega_M = 0.3$, $\Omega_\Lambda = 0.7$).

We find a weak trend of a $L - Z/Z_\odot$ relation for the high redshift quasars. Due to the scatter in metallicity and the small range of covered luminosity the probability for a correlation by chance is $\sim 6\,\%$. However, the trend is in good agreement with results obtained for quasars at lower redshift (Hamann & Ferland 1999) and for composite spectra based on a large quasar sample, which we are currently investigating (Dietrich et al. 2002b; Warner et al. 2003).

We are grateful to our colleagues J.A. Baldwin, G.J. Ferland, and K.T. Korista for helpful discussions. We thank Fred Chaffee and Craig Foltz for support and help with the MMT observations. MD thanks Katherine L. Wu for comments on the manuscript. MD and FH acknowledge support from NASA grant NAG 5-3234 and NSF grant AST-99-84040 (University of Florida). MV gratefully acknowledges financial support from the Columbus Fellowship.

REFERENCES

Allende Prieto, C., Lambert, D.L., & Asplund, M. 2001, ApJ, 556, L63

Allende Prieto, C., Lambert, D.L., & Asplund, M. 2002, ApJ, 573, L137

Anderson, S.F., et al. 2001, AJ, 122, 503

Andreani, P., La Franca, F., & Cristiani, S. 1993, MNRAS, 261, L35

Arimoto, N. & Yoshii, Y. 1987, A&A, 173, 23

Baldwin, J.A. & Netzer, H. 1978, ApJ, 226, 1

Baldwin, J.A., et al. 2002, ApJ, in press

Becker, R.H., et al. 2001, AJ, 122, 2850

Bevington, P.R. 1969, Data Reduction and Error Analysis for the Physical Science, McGraw-Hill, Inc.

Bica, E., Arimoto, N., & Alloin, D. 1988, A&A, 202, 8

Boyle, B.J. & Terlevich, R.J. 1998, MNRAS, 293, L49

Carilli, C.L., Bertoldi, F., Omont, A., Cox, P., McMahon, R.G., & Isaak, K.G. 2001, AJ, 122, 1679

Carilli, C.L., et al. 2000, ApJ, 533, L13

Carroll, S.M., Press, W.H., & Turner, E.L. 1992, ARA&A, 30, 499

Cen, R. & Ostriker, J.P. 1999, ApJ, 519, L109

Connolly, A.J., Szalay, A.S., Dickinson, M., Subbarao, M., & Brunner, R.J. 1997, ApJ, 486, L11

Constantin, A., Shields, J.C., Hamann, F., Foltz, C.B., & Chaffee, F.H. 2002, ApJ, 565, 50

Davidson, K. 1977, ApJ, 218, 20

Dickinson, M. 1998, in "The Hubble Deep Field", STScI Symp., eds. M. Livio, S. Fall, & P. Madau, p.219

Dietrich, M., Appenzeller, I., Wagner, S.J., et al. 1999, A&A, 352, L1

Dietrich, M., et al. 2002a, A&A, in press

Dietrich, M., et al. 2002b, ApJ, 581, 912

Dietrich, M. & Hamann, F. 2003, in prep.

Dietrich, M. & Wilhelm-Erkens, U. 2000, A&A, 354, 17

Djorgovski, G. 2002, http://www.astro.caltech.edu/∼george/z4.qsos

Faber, S.M. 1973, ApJ, 179, 731

Fan, X., et al. 1999, AJ, 118, 1

Fan, X., et al. 2000a, AJ, 119, 1

Fan, X., et al. 2000b, AJ, 120, 1167

Fan, X., et al. 2001, AJ, 122, 2833

Fan, X., Narayanan, V.K., Strauss, M.A., White, R.L., Becker, R.H., Pentericci, L., & Rix, H.-W. 2002, AJ, 123, 1247

Ferland, G.J., Baldwin, J.A., Korista, K.T., Hamann, F., Carswell, R.F., Phillips, M., Wilkes, B., & Williams, R.E. 1996, ApJ, 461, 683

Ferland, G.J., Korista, K.T., Verner, D.A., Ferguson, J.W., Kingdon, J.B., & Verner, E.M. 1998, PASP, 110, 761

Ferrarese, L. & Merritt, D. 2001, ApJ, 555, L79

Friaça, A.C.S. & Terlevich, R.J. 1998, MNRAS, 298, 399

Gallego, J. Zamorano, J., Aragon-Salamenca, A., & Rego, M. 1995, ApJ, 455, L1

Gaskell, C.M., Shields, G.A., & Wampler, E.J. 1981, ApJ, 249, 443

Gebhardt, K., et al. 2000, ApJ, 543, L5

Gnedin, N.Y. & Ostriker, J.P. 1997, ApJ, 486, 581

Granato, G.L., Silva, L., Monaco, P., Panuzzo, P., Salucci, P., De Zotti, G., & Danese, L. 2001, MNRAS, 324, 757

Grandi, S.A. 1982, ApJ, 255, 25

Grevesse, N. & Sauval, A.J. 1998, Space Sci.Rev., 85, 161

Haehnelt, M.G. & Kauffmann, G. 2000, MNRAS, 318, L35

Haiman, Z. & Loeb, A. 1998, ApJ, 503, 505

Hamann, F. 1997, ApJS, 109, 279

Hamann, F. & Ferland, G.J. 1992, ApJ, 381, L53

Hamann, F. & Ferland, G.J. 1993, ApJ, 418, 11

Hamann, F. & Ferland, G.J. 1999, ARA&A, 37, 487

Hamann, F. & Korista, K.T. 1996, ApJ, 464, 158

Hamann, F., Korista, K.T., Ferland, G.J., Warner, C., & Baldwin, J.A. 2002, ApJ, 564, 592

Hamann, F., Korista, K.T., & Morris, S.L. 1993, ApJ, 415, 541

Henry, R.B.C., Edmunds, M.G., & Köppen, J. 2000, ApJ, 541, 660

Holweger, 2001, in Joint SOHO/ACE workshop "Solar and Galactic Composition", ed. R.F. Wimmer-Schweingruber, AIP Conf.Proc. Vol. 598, p.23

Isaak, K.G., McMahon, R.G., Hils, R.E., & Withington, S. 1994, MNRAS, 269, L28

Izotov, Y.I. & Thuan, T.X. 1999, ApJ, 511, 639

Kauffmann, G. & Haehnelt, M.G. 2000, MNRAS, 311, 576

Kobulnicky, H.A. & Skillman, E.D. 1996, ApJ, 471, 211

Kormendy, J. & Richstone, D. 1995, ARA&A, 33, 581

Krolik, J.H. & Voit, G.M. 1998, ApJ, 497, L5

Lanzetta, K.M., Yahata, N., Pascarelle, S., Chen, H.-W., Fernandez-Soto, A. 2002, ApJ, 570, 492

Laor, A., et al. 1994, ApJ, 420, 110

Laor, A., Fiore, F., Elvis, M., Wilkes, B.J., & McDowell, J.C. 1997, ApJ, 477, 93

Lilly, S.J., Le Fèvre, O., Hammer, F., & Crampton, D. 1996, ApJ, 460, L1

Madau, P., Ferguson, H.C., Dickinson, M.E., Giavalisco, M., Steidel, C.C., & Fruchter, A. 1996, MNRAS, 283, 1388

Magorrian, J., Tremaine, S., & Richstone, D. 1998, AJ, 115, 2285

Mathews, W.G. & Ferland, G.J. 1987, ApJ, 323, 456

Matteucci, F. 1992, ApJ, 397, 32

Matteucci, F. & Padovani, P. 1993, ApJ, 419, 485

Merritt, D. & Ferrarese, L. 2001, ApJ, 547, 140

Møller, P., Jakobson, P. & Perryman, M.A. 1994, A&A, 287, 719

Nolan, L.A., Dunlop, J.S., & Jimenez, R. 2001, MNRAS, 323, 385

Omont, A., Cox, P., Bertoldi, F., McMahon, R.G., Carilli, C., & Isaak, K.G. 2001, A&A, 374, 371

Omont, A., McMahon, R.G., Cox, P., Kreysa, E., Bergeron, J., Pajot, F., & Storrie-Lombardi, L.J. 1996, A&A, 315, 1

Osmer, P.S. 1980, ApJ, 237, 666

Osmer, P.S., Porter, A.C., Green, R.F. 1994, ApJ, 436, 678

Padovani, P. & Matteucci, F. 1993, ApJ, 416, 26

Pagel, B.E.J. & Edmunds, M.G. 1981, ARA&A, 19, 77

Petitjean, P., Rauch, M., & Carswell, R.F. 1994, A&A, 291, 29

Pettini, M. 1999, in Proc.of ESO Workshop "Chemical Evolution from Zero to High Redshift", ed. J. Walsh & M. Rosa, LNP, p.233

Pettini, M., Kellogg, M., Steidel, C.C., Dickinson, M., Adelberger, K.L., & Giavalisco, M. 1998, ApJ, 508, 539

Pettini, M., Ellison, S.L., Bergeron, J., & Petitjean, P. 2002, A&A, 391, 21

Richstone, D., et al. 1998, Nature, 395 A, 14

Romano, D., Silva, L., Matteucci, F., & Danese, L. 2002, MNRAS, 334, 444

Sandage, A.R. 1972, ApJ, 176, 21

Sargent, W.L.W., Boksenberg, A., & Steidel, C.C. 1988, ApJS, 68, 539

Sargent, W.L.W., Steidel, C.C., & Boksenberg, A. 1989, ApJS, 69, 703

Schneider, D.P., Schmidt, M., & Gunn, J.E. 1991a, AJ, 101, 2004

Schneider, D.P., Schmidt, M., & Gunn, J.E. 1991b, AJ, 102, 837

Sharp, R.G., McMahon, R.G., Irwin, M.J., & Hodgkin, S.T. 2001, MNRAS, 326, L45

Shemmer, O. & Netzer, H. 2002, ApJ, 567, L19

Shields, G.A. 1976, ApJ, 204, 330

Steidel, C.C., Adelberger, K.L., Giavalisco, M., Dickinson, M., & Pettini, M. 1999, ApJ, 519, 1

Stern, D., et al. 2000, ApJ, 533, L75

Storrie-Lombardi, L.J., McMahon, R.G., Irwin, M.J., & Hazard, C. 1996, ApJ, 468, 121

Storey, P.J. & Hummer, D.G. 1995, MNRAS, 272, 41

Surdej, J. & Hutsemeker, D. 1987, A&A, 177, 42

Telfer, R.C., Zheng, W., Kriss, G.A., & Davidsen, A.F. 2002, ApJ, 565, 773

Tinsley, B.M. 1980, Fundam. Cosmic Phys., 5, 287

Tremaine, S., et al. 2002, ApJ, 574, 740

Tresse, L. & Maddox, S.J. 1998, ApJ, 495, 691

Uomoto, A. 1984, ApJ, 284, 497

van Zee, L., Salzer, J.J., & Haynes, M.P. 1998, ApJ, 497, L1

Verner, E.M., Verner, D.A., Korista, K.T., Ferguson, J.W., Hamann, F., & Ferland, G.J. 1999, ApJS, 120, 101

Vestergaard, M. & Wilkes, B.J. 2001, ApJS, 134, 1

Warner, C., Hamann, F., Shields, J.C., Constantin, A., Foltz, C.B., & Chaffee, F.H. 2002, ApJ, 567, 68

Warner, C., et al. 2003, ApJ, in prep.

Weymann, R.J., Morris, S.L., Foltz, C.B., & Hewett, P.C. 1991, ApJ, 373, 23

Zheng, W., Kriss, G.A., Telfer, R.C., Grimes, J.P., & Davidson, A.F. 1997, ApJ, 475, 469

Zheng, W., et al. 2000, AJ, 120, 1607

This 2-column preprint was prepared with the AAS LaTeX macros v5.0.

Fig. 1.— (a) Example of the reconstruction of the Lyα, N Vλ1240 emission line profile complex for PSSJ 0248+1802 (thick line). The individual profiles are displayed as solid lines while the broad and narrow components are shown as dotted lines. The sum of the profile fits of the individual lines is plotted as long dashed line. The residuum is shown at the bottom of the figure which is calculated by subtracting the individual profile fits from the power-law continuum corrected quasar spectrum. The short dashed line indicates the zero-level for the residuum. (b) Example of the reconstruction of the C IVλ1549, He IIλ1640, O III]λ1663 emission line profile complex for PSSJ 0248+1802; line types are the same as those shown in (a). (c) Example of the reconstruction of the He IIλ1640, O III]λ1663, and N III]λ1750 emission line profile complex for BRI 1328-0433; line types are the same as those shown in (a).

Fig. 2.— The metallicities derived from several emission line ratios are shown for the individual high redshift quasars as a function of redshift.

Fig. 3.— Comparison of the metallicity estimates for each quasar based on N III]/O III] versus N V/C IV (a), N V/O VI (b), N V/(O VI+C IV) (c), and N V/He II (d).

Fig. 4.— Same as Figure 3 for N V]/C IV versus N V/O VI (a) , N V/(O VI+C IV) (b), N V/He II (c), and N IV]/O III] (d).

Fig. 5.— Same as Figure 3 for N IV]/C IV versus N V/C IV (a) and N III/O III] (b). The comparison of the metallicity given by N IV]/O III] versus N III]/O III] is shown in the lower left panel (c).

Fig. 6.— (a) – Comparison of the metallicities for each quasar based on the mean metallicity obtained by the line ratios using N V versus the line ratios using inter-combination lines. (b) – The comparison of the mean metallicities computed without using N V/He II, and N IV]/C IV and N III]/C III].

Fig. 7.— The average metallicities of the individual high redshift quasars as a function of redshift. The dotted line marks solar metallicity $Z_{\odot}$.

Fig. 8.— The average metallicities of the individual high redshift quasars as a function of rest-frame continuum luminosity L_{λ}(1450Å). The dotted line marks solar metallicity $Z_{\odot}$. The dashed line displays the least squares fit to the measurements.

TABLE 1

THE HIGH REDSHIFT QUASAR SAMPLE

quasar	λλ range [Å]	z	log L_λ[a]	ref.[b]	quasar	λλ range [Å]	z	log L_λ[a]	ref.[b]
Q 0000-263	671 – 1862	4.11	45.20	6	PC 1158+4635	788 – 1655	4.73	44.23	6
PSSJ 0003+2730	1072 – 1769	4.24	43.65	1	Q 1159+123	706 – 1550	3.50	44.24	7,9
BR 0019-1522	663 – 1773	4.53	43.76	1,4	BR 1202-0725	631 – 1758	4.69	44.04	1,4
PC 0027+0525	1104 – 1846	4.10	42.49	1	Q 1208+1011	660 – 1600	3.80	44.56	7
PC 0027+0521	1078 – 1805	4.22	42.47	1	PC 1233+4752	884 – 1744	4.45	43.20	6
SDSS 0032+0040	1003 – 1663	4.75	43.03	1	PC 1247+3406	764 – 1609	4.90	43.71	6
Q 0046-293	844 – 2054	4.01	43.60	3	PKS 1251-407	778 – 1707	4.47	43.32	3
Q 0046-282	763 – 1989	3.83	43.92	2	PC 1301+4747	887 – 1915	4.00	42.57	1,6
PSSJ 0059+0003	1056 – 1871	4.16	43.46	1	PSSJ 1317+3531	1014 – 1800	4.37	43.67	1
Q 0101-304	831 – 2000	4.07	43.59	3	BRI 1328-0433	676 – 1858	4.20	43.62	1,4
BRI 0103+0032	653 – 1801	4.44	43.83	1,4	Q 1330+0108	702 – 1549	3.51	43.93	7
PC 0104+0215	836 – 1835	4.17	43.23	6	APM 1335-0417	798 – 1722	4.38	43.56	3,4
PC 0131+0120	900 – 1937	3.79	43.78	1,6	BRI 1346-0322	702 – 1923	3.99	43.61	1,4
PSSJ 0152+0735	1113 – 1863	4.05	43.27	1	Q 1422WOWccs02	828 – 1808	3.59	42.13	8
BRI 0151-0025	670 – 1858	4.19	43.72	1,4	PC 1450+3404	1110 – 1840	4.20	42.91	1
BRI 0241-0146	721 – 1950	4.06	43.80	1,4	BRI 1500+0824	879 – 1942	3.95	43.49	1,3,4
BR 0245-0608	711 – 1661	4.22	43.87	4	GB 1508+5714	661 – 1654	4.30	44.09	4
PSSJ 0248+1802	1003 – 1778	4.44	44.08	1	PC 1548+4637	950 – 2090	3.54	43.81	6
PC 0307+0222	811 – 1747	4.39	43.67	1,6	BRI 1557+0313	747 – 2019	3.89	43.21	3,4
SDSS 0338-0021	1056 – 1718	5.00	43.45	2	PSSJ 1618+4125	1108 – 1836	4.21	43.37	1
PC 0345+0130	933 – 2046	3.64	42.98	6	PC 1640+4628	919 – 2016	3.71	43.22	6
BR 0351-1034	679 – 1616	4.35	43.87	4	PC 1643+465A	902 – 1950	3.79	42.94	6
BR 0401-1711	673 – 1876	4.23	43.74	1,4	PC 1640+465B	892 – 1963	3.83	42.81	6
PC 0751+5623	869 – 1794	4.28	43.82	6	GB 1745+6227	694 – 1973	3.89	43.72	1,4
PC 0910+5625	876 – 1801	4.04	43.25	6	RX 1759.4+6638	1083 – 1756	4.33	43.78	1
BR 0951-0450	661 – 1833	4.37	43.76	1,4	Q 2000-330	703 – 1574	3.78	44.10	5
BRI 0952-0115	681 – 1776	4.43	43.88	1,4	PC 2047+0123	902 – 1978	3.80	43.27	6
PC 0953+4749	866 – 1743	4.46	43.69	6	Q 2133-4311	833 – 1798	4.18	42.82	3
BRI 1013+0035	660 – 1785	4.41	43.84	1,4	Q 2133-4625	829 – 1974	4.18	42.78	3
BR 1033-0327	636 – 1782	4.51	44.02	1,4	Q 2134-4521	805 – 1732	4.37	43.15	3
BRI 1050-0000	666 – 1784	4.29	44.14	1,4	Q 2203+292	865 – 1770	4.40	43.28	1,6
PSSJ 1057+4555	1039 – 1865	4.11	43.97	1	BR 2212-1626	706 – 1932	4.00	43.88	1,4
BRI 1108-0747	734 – 1938	3.92	43.90	1,4	BR 2237-0607	682 – 1758	4.56	44.18	1,3,4
BRI 1110+0106	714 – 1957	3.92	43.80	1,4	BR 2248-1242	706 – 1899	4.16	43.85	1,4
BRI 1114-0822	654 – 1598	4.50	44.10	4	PC 2331+0216	855 – 1944	4.09	43.43	1,3,6

[a] $\log L_\lambda$ refers to the continuum luminosity $L_\lambda(1450\text{Å})$ in $\mathrm{erg\,s^{-1}\,Å^{-1}}$

[b] 1 - Constantin et al. 2002; 2 - Dietrich et al. 1999; 3 - Dietrich et al. 2002a; 4 - Storrie-Lombardi et al. 1996; 5 - Sargent et al. 1989; 6 - Schneider et al. 1991a,b; 7 - Steidel & Sargent, priv.comm.; 8 - Steidel, priv.comm.; and 9 - Sargent et al. 1988

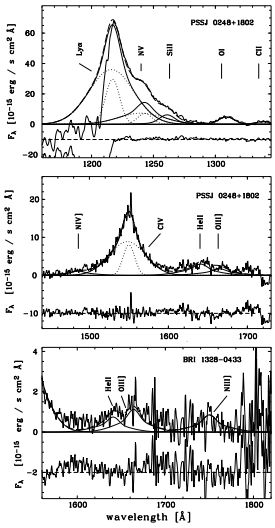
PSSJ 0248+1802
Lyα
NV
SiII
OI
CII
PSSJ 0248+1802
NIV]
CIV
HeII
OIII]
BRI 1328−0433
HeII
OIII]
NIII]
wavelength [Å]

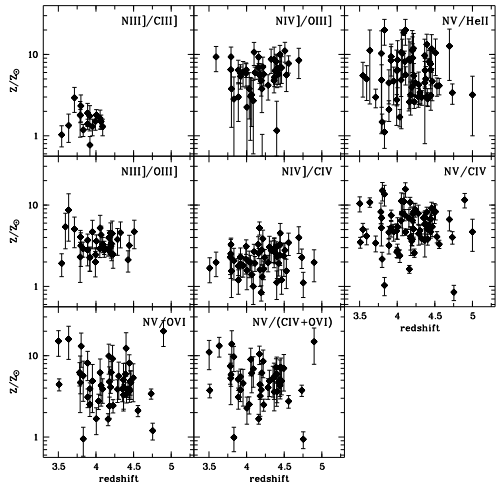
NIII]/CIII]
NIV]/OIII]
NV/HeII
NIII]/OIII]
NIV]/CIV
NV/CIV
NV/OVI
NV/(CIV+OVI)
redshift

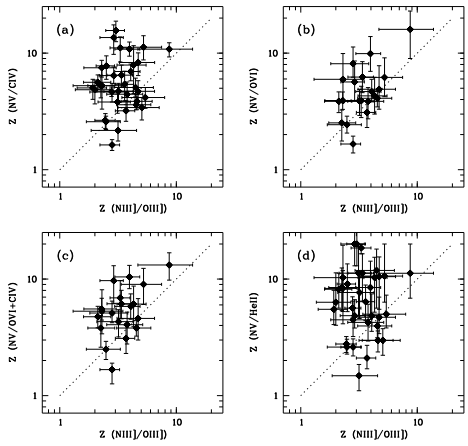
(a)
(b)
(c)
(d)
Z (NV/CIV)
Z (NV/OVI)
Z (NV/OVI+CIV)
Z (NV/HeII)
Z ([NIII]/[OIII])

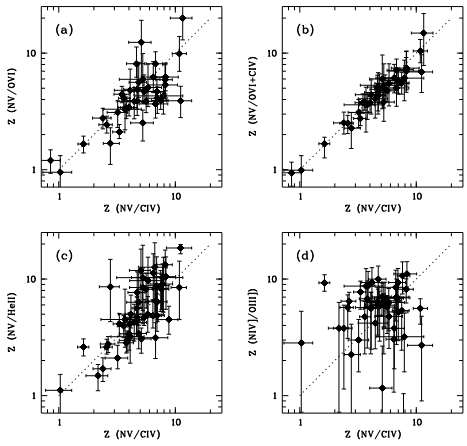
(a)
(b)
(c)
(d)
Z (NV/OVI)
Z (NV/OVI+CIV)
Z (NV/HeII)
Z (NIV]/[OIII])
Z (NV/CIV)

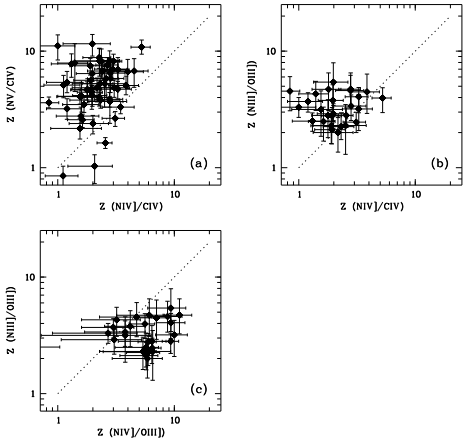
Z (NV/CIV)
Z (NIV]/CIV)
(a)
Z (NIII]/OIII])
Z (NIV]/CIV)
(b)
Z (NIII]/OIII])
Z ([IIIO/[NIV])
(c)

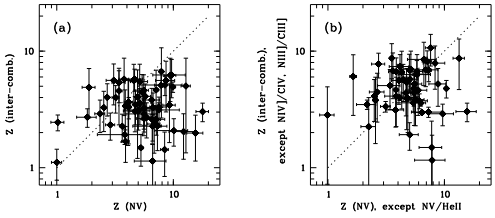
Z (inter-comb.)
Z (NV)
(a)
Z (inter-comb.), except NIV]/CIV, NIII]/CIII]
Z (NV), except NV/HeII
(b)

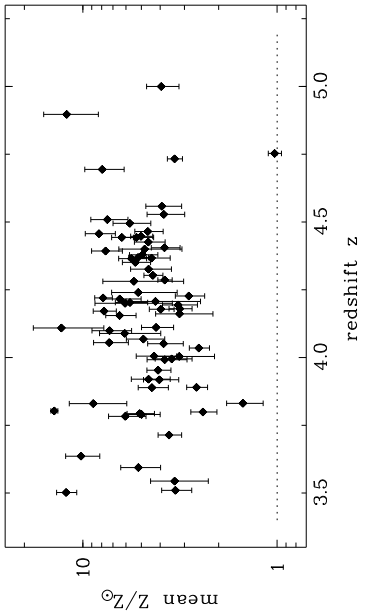
mean Z/Z⊙
10
1
3.5
4.0
4.5
5.0
redshift z

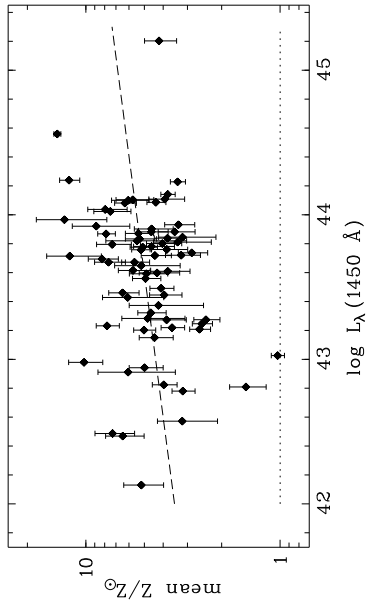
mean Z/Z⊙
10
1
42
43
44
45
log L_λ(1450 Å)

TABLE 2

MEAN METALLICITIES BASED ON THE INDIVIDUAL EMISSION LINE RATIOS. THE NUMBER OF QUASARS FOR WHICH THE INDIVIDUAL LINE RATIOS ARE AVAILABLE IS GIVEN IN COLUMN (2). THE MEAN METALLICITIES WE DERIVED FOR THE SCATTERED LIGHT CORRECTED N Vλ1240 AND C IVλ1549 EMISSION ARE GIVEN IN COLUMN (5).

ratio (1)	n (2)	mean (3)	median (4)	mean$_{corr}$ (5)
N III]λ1750/C III]λ1909	17	1.6 ± 0.2	1.5	···
N III]λ1750/O III]λ1663	35	3.6 ± 0.3	3.2	···
N IV]λ1486/C IVλ1549	54	2.3 ± 0.2	2.2	2.6 ± 0.2
N IV]λ1486/O III]λ1663	46	6.0 ± 0.5	6.0	···
N Vλ1240/He IIλ1640	61	6.8 ± 0.8	5.5	4.0 ± 0.6
N Vλ1240/C IVλ1549	70	6.1 ± 0.4	5.3	4.6 ± 0.4
N Vλ1240/O VIλ1034	47	5.6 ± 0.7	4.4	3.5 ± 0.5
N Vλ1240/(O VI+C IV)	47	5.7 ± 0.6	5.1	4.0 ± 0.5
all ratios	70	5.3 ± 0.3	4.7	···
inter-combination lines	62	3.6 ± 0.3	3.3	···
N V-ratios	70	6.2 ± 0.4	5.6	···